

Supplementary Materials to ‘‘Multi-channel Weighted Nuclear Norm Minimization for Real Color Image Denoising’’

Jun Xu¹, Lei Zhang^{1,*}, David Zhang¹, and Xiangchu Feng²

¹Dept. of Computing, The Hong Kong Polytechnic University, Hong Kong, China

²School of Mathematics and Statistics, Xidian University, Xi'an, China

{csjunxu, cslzhang, csdzhang}@comp.polyu.edu.hk, xcfeng@mail.xidian.edu.cn

In this supplementary file, we provide:

1. The proof of the Theorem 1 in the main paper;
2. More denoising results on the Kodak PhotoCD dataset;
3. More visual comparisons of denoised images on the real noisy images of dataset [1];
4. More visual comparisons of denoised images on the real noisy images of dataset [2].

1. Proof of Theorem 1.

Theorem 1. Assume that the weights in \mathbf{w} are in a non-descending order, the sequence $\{\mathbf{X}_k\}$, $\{\mathbf{Z}_k\}$, and $\{\mathbf{A}_k\}$ generated in Algorithm 1 satisfy:

$$(a) \lim_{k \rightarrow \infty} \|\mathbf{X}_{k+1} - \mathbf{Z}_{k+1}\|_F = 0; \quad (b) \lim_{k \rightarrow \infty} \|\mathbf{X}_{k+1} - \mathbf{X}_k\|_F = 0; \quad (c) \lim_{k \rightarrow \infty} \|\mathbf{Z}_{k+1} - \mathbf{Z}_k\|_F = 0. \quad (1)$$

Proof. 1. Firstly, we prove that the sequence $\{\mathbf{A}_k\}$ generated by Algorithm 1 is upper bounded. Let $\mathbf{X}_{k+1} + \rho_k^{-1} \mathbf{A}_k = \mathbf{U}_k \boldsymbol{\Sigma}_k \mathbf{V}_k^\top$ be its singular value decomposition (SVD) [3] in the $(k+1)$ -th iteration. According to Corollary 1 of [4], we can have the SVD of \mathbf{Z}_{k+1} as $\mathbf{Z}_{k+1} = \mathbf{U}_k \hat{\boldsymbol{\Sigma}}_k \mathbf{V}_k^\top = \mathbf{U}_k \mathcal{S}_{\frac{\mathbf{w}}{\rho_k}}(\boldsymbol{\Sigma}_k) \mathbf{V}_k^\top$. Then we have

$$\|\mathbf{A}_{k+1}\|_F = \|\mathbf{A}_k + \rho_k (\mathbf{X}_{k+1} - \mathbf{Z}_{k+1})\|_F = \rho_k \|\rho_k^{-1} \mathbf{A}_k + \mathbf{X}_{k+1} - \mathbf{Z}_{k+1}\|_F \quad (2)$$

$$= \rho_k \|\mathbf{U}_k \boldsymbol{\Sigma}_k \mathbf{V}_k^\top - \mathbf{U}_k \mathcal{S}_{\frac{\mathbf{w}}{\rho_k}}(\boldsymbol{\Sigma}_k) \mathbf{V}_k^\top\|_F = \rho_k \|\boldsymbol{\Sigma}_k - \mathcal{S}_{\frac{\mathbf{w}}{\rho_k}}(\boldsymbol{\Sigma}_k)\|_F \quad (3)$$

$$= \rho_k \sqrt{\sum_i (\boldsymbol{\Sigma}_k^{ii} - \mathcal{S}_{\frac{\mathbf{w}_i}{\rho_k}}(\boldsymbol{\Sigma}_k^{ii}))^2} \leq \rho_k \sqrt{\sum_i \left(\frac{\mathbf{w}_i}{\rho_k}\right)^2} = \sqrt{\sum_i w_i^2}. \quad (4)$$

The inequality in the second last step can be proved as follows: given the diagonal matrix $\boldsymbol{\Sigma}_k$, we define $\boldsymbol{\Sigma}_k^{ii}$ as the i -th element of $\boldsymbol{\Sigma}_k$. If $\boldsymbol{\Sigma}_k^{ii} \geq \frac{\mathbf{w}_i}{\rho_k}$, we have $\mathcal{S}_{\frac{\mathbf{w}_i}{\rho_k}}(\boldsymbol{\Sigma}_k^{ii}) = \boldsymbol{\Sigma}_k^{ii} - \frac{\mathbf{w}_i}{\rho_k}$. If $\boldsymbol{\Sigma}_k^{ii} < \frac{\mathbf{w}_i}{\rho_k}$, we have $\mathcal{S}_{\frac{\mathbf{w}_i}{\rho_k}}(\boldsymbol{\Sigma}_k^{ii}) = 0$. Overall, we have $|\boldsymbol{\Sigma}_k^{ii} - \mathcal{S}_{\frac{\mathbf{w}_i}{\rho_k}}(\boldsymbol{\Sigma}_k^{ii})| \leq \frac{\mathbf{w}_i}{\rho_k}$ and hence the inequality holds. Hence, the sequence $\{\mathbf{A}_k\}$ is upper bounded.

2. Secondly, we prove that the sequence of Lagrangian function $\{\mathcal{L}(\mathbf{X}_{k+1}, \mathbf{Z}_{k+1}, \mathbf{A}_k, \rho_k)\}$ is also upper bounded. Since we have the globally optimal solution of \mathbf{X} and \mathbf{Z} in their corresponding subproblems, we always have

$$\mathcal{L}(\mathbf{X}_{k+1}, \mathbf{Z}_{k+1}, \mathbf{A}_k, \rho_k) \leq \mathcal{L}(\mathbf{X}_k, \mathbf{Z}_k, \mathbf{A}_k, \rho_k). \quad (5)$$

Based on the updating rule that $\mathbf{A}_{k+1} = \mathbf{A}_k + \rho_k (\mathbf{X}_{k+1} - \mathbf{Z}_{k+1})$, we have

$$\mathcal{L}(\mathbf{X}_{k+1}, \mathbf{Z}_{k+1}, \mathbf{A}_{k+1}, \rho_{k+1}) \quad (6)$$

$$= \mathcal{L}(\mathbf{X}_{k+1}, \mathbf{Z}_{k+1}, \mathbf{A}_k, \rho_k) + \langle \mathbf{A}_{k+1} - \mathbf{A}_k, \mathbf{X}_{k+1} - \mathbf{Z}_{k+1} \rangle + \frac{\rho_{k+1} - \rho_k}{2} \|\mathbf{X}_{k+1} - \mathbf{Z}_{k+1}\|_F^2 \quad (7)$$

$$= \mathcal{L}(\mathbf{X}_{k+1}, \mathbf{Z}_{k+1}, \mathbf{A}_k, \rho_k) + \frac{\rho_{k+1} + \rho_k}{2\rho_k^2} \|\mathbf{A}_{k+1} - \mathbf{A}_k\|_F^2. \quad (8)$$

*This work is supported by HK RGC GRF grant (PolyU 5313/13E) and China NSFC grant (no. 61672446).

Since the sequence $\{\mathbf{A}_k\}$ is upper bounded, the sequence $\{\mathbf{A}_{k+1} - \mathbf{A}_k\}$ is also upper bounded. Denote by a the upper bound of $\{\mathbf{A}_{k+1} - \mathbf{A}_k\}$, i.e., $\|\mathbf{A}_{k+1} - \mathbf{A}_k\|_F \leq a$ holds for $\forall k \geq 0$, we have

$$\mathcal{L}(\mathbf{X}_{k+1}, \mathbf{Z}_{k+1}, \mathbf{A}_{k+1}, \rho_{k+1}) \leq \mathcal{L}(\mathbf{X}_1, \mathbf{Z}_1, \mathbf{A}_0, \rho_0) + a^2 \sum_{k=0}^{\infty} \frac{\rho_{k+1} + \rho_k}{2\rho_k^2} \quad (9)$$

$$= \mathcal{L}(\mathbf{X}_1, \mathbf{Z}_1, \mathbf{A}_0, \rho_0) + a^2 \sum_{k=0}^{\infty} \frac{\mu + 1}{2\mu^k \rho_0} \quad (10)$$

$$\leq \mathcal{L}(\mathbf{X}_1, \mathbf{Z}_1, \mathbf{A}_0, \rho_0) + \frac{a^2}{\rho_0} \sum_{k=0}^{\infty} \frac{1}{\mu^{k-1}}. \quad (11)$$

The last inequality holds since $\mu > 1$ and $\mu + 1 < 2\mu$. Therefore, we have $\sum_{k=0}^{\infty} \frac{1}{\mu^{k-1}} < \infty$ and the sequence of Lagrangian function $\{\mathcal{L}(\mathbf{X}_{k+1}, \mathbf{Z}_{k+1}, \mathbf{A}_{k+1}, \rho_{k+1})\}$ is upper bounded.

3. Thirdly, we prove that the sequences of $\{\mathbf{X}_k\}$ and $\{\mathbf{Z}_k\}$ are upper bounded. Since

$$\|\mathbf{W}(\mathbf{Y} - \mathbf{X}_k)\|_F^2 + \|\mathbf{Z}_k\|_{\mathbf{w},*} = \mathcal{L}(\mathbf{X}_k, \mathbf{Z}_k, \mathbf{A}_{k-1}, \rho_{k-1}) - \langle \mathbf{A}_{k-1}, \mathbf{X}_k - \mathbf{Z}_k \rangle - \frac{\rho_{k-1}}{2} \|\mathbf{X}_k - \mathbf{Z}_k\|_F^2 \quad (12)$$

$$= \mathcal{L}(\mathbf{X}_k, \mathbf{Z}_k, \mathbf{A}_{k-1}, \rho_{k-1}) + \frac{1}{2\rho_{k-1}} (\|\mathbf{A}_{k-1}\|_F^2 - \|\mathbf{A}_k\|_F^2), \quad (13)$$

both $\{\mathbf{W}(\mathbf{Y} - \mathbf{X}_k)\}$ and $\{\mathbf{Z}_k\}$ are upper bounded, and hence the sequence $\{\mathbf{X}_k\}$ is bounded by the Cauchy-Schwarz inequality and triangle inequality. We can obtain that

$$\lim_{k \rightarrow \infty} \|\mathbf{X}_{k+1} - \mathbf{Z}_{k+1}\|_F = \lim_{k \rightarrow \infty} \rho_k^{-1} \|\mathbf{A}_{k+1} - \mathbf{A}_k\|_F = 0, \quad (14)$$

and the equation (a) is proved.

4. Then we can prove that

$$\lim_{k \rightarrow \infty} \|\mathbf{X}_{k+1} - \mathbf{X}_k\|_F = \lim_{k \rightarrow \infty} \|(\mathbf{W}^\top \mathbf{W} + \frac{\rho_k}{2} \mathbf{I})^{-1} (\mathbf{W}^\top \mathbf{W} \mathbf{Y} - \mathbf{W}^\top \mathbf{W} \mathbf{Z}_k - \frac{1}{2} \mathbf{A}_k) - \rho_{k-1}^{-1} (\mathbf{A}_k - \mathbf{A}_{k-1})\|_F \quad (15)$$

$$\leq \lim_{k \rightarrow \infty} \|(\mathbf{W}^\top \mathbf{W} + \frac{\rho_k}{2} \mathbf{I})^{-1} (\mathbf{W}^\top \mathbf{W} \mathbf{Y} - \mathbf{W}^\top \mathbf{W} \mathbf{Z}_k - \frac{1}{2} \mathbf{A}_k)\|_F + \rho_{k-1}^{-1} \|\mathbf{A}_k - \mathbf{A}_{k-1}\|_F \quad (16)$$

$$= 0, \quad (17)$$

and hence the equation (b) is proved.

5. Finally, the equation (c) can be proved by checking that

$$\lim_{k \rightarrow \infty} \|\mathbf{Z}_{k+1} - \mathbf{Z}_k\|_F = \lim_{k \rightarrow \infty} \|\mathbf{X}_k + \rho_{k-1}^{-1} \mathbf{A}_{k-1} - \mathbf{Z}_k + \mathbf{X}_{k+1} - \mathbf{X}_k - \rho_{k-1}^{-1} \mathbf{A}_{k-1} + \rho_k^{-1} \mathbf{A}_k - \rho_k^{-1} \mathbf{A}_{k+1}\|_F \quad (18)$$

$$\leq \lim_{k \rightarrow \infty} (\|\Sigma_{k-1} - \mathcal{S}_{\mathbf{w}/\rho_{k-1}}(\Sigma_{k-1})\|_F + \|\mathbf{X}_{k+1} - \mathbf{X}_k\|_F + \|\rho_{k-1}^{-1} \mathbf{A}_{k-1} + \rho_k^{-1} \mathbf{A}_{k+1} - \rho_k^{-1} \mathbf{A}_k\|_F) \quad (19)$$

$$\leq \lim_{k \rightarrow \infty} (\rho_{k-1}^{-1} \|\mathbf{w}\|_F + \|\mathbf{X}_{k+1} - \mathbf{X}_k\|_F + \|\rho_{k-1}^{-1} \mathbf{A}_{k-1} + \rho_k^{-1} \mathbf{A}_{k+1} - \rho_k^{-1} \mathbf{A}_k\|_F) \quad (20)$$

$$= 0, \quad (21)$$

where $\mathbf{U}_{k-1} \Sigma_{k-1} \mathbf{V}_{k-1}^\top$ is the SVD of the matrix $\mathbf{X}_k + \rho_{k-1}^{-1} \mathbf{A}_{k-1}$. \square

2. More denoising results on the Kodak PhotoCD dataset

In the main paper, we have given the PSNR results of the competing methods on the 24 high quality images from the Kodak PhotoCD dataset when the standard deviations of the additive white Gaussian noise (AWGN) are $\sigma_r = 40, \sigma_g = 20, \sigma_b = 30$ for R, G, B channels, respectively. Here we provide more denoising results on this dataset. In Tables 1-3, we give the PSNR results on these images when the noise standard deviations are $\sigma_r = 40, \sigma_g = 20, \sigma_b = 30$ in Table 1, $\sigma_r = 30, \sigma_g = 10, \sigma_b = 50$ in Table 2 and $\sigma_r = 5, \sigma_g = 30, \sigma_b = 15$ in Table 3, respectively. In Figures 1-6, we give the visual comparisons of the denoised images by different methods.

Table 1. PSNR(dB) results of different denoising methods on the Kodak PhotoCD dataset.

	$\sigma_r = 40, \sigma_g = 20, \sigma_b = 30$									
Image#	CBM3D [5]	MLP [6]	TNRD [7]	DnCNN [8]	NI [9]	NC [10]	WNNM-1 [11]	WNNM-2	WNNM-3	MC-WNNM
1	25.24	25.70	25.74	20.47	23.85	24.90	26.01	25.95	25.58	26.66
2	28.27	30.12	30.21	20.47	25.90	25.87	30.08	30.11	29.80	30.20
3	28.81	31.19	31.49	20.53	26.00	28.58	31.58	31.61	31.20	32.25
4	27.95	29.88	29.86	20.47	25.82	25.67	30.13	30.16	29.84	30.49
5	25.03	26.00	26.18	20.52	24.38	25.15	26.44	26.39	25.32	26.82
6	26.24	26.84	26.90	20.66	24.65	24.74	27.39	27.30	26.88	27.98
7	27.88	30.28	30.40	20.52	25.63	27.69	30.47	30.54	29.70	30.98
8	25.05	25.59	25.83	20.57	24.02	25.30	26.71	26.75	25.26	26.90
9	28.44	30.75	30.81	20.50	25.94	27.44	30.86	30.92	30.29	31.49
10	28.27	30.38	30.57	20.52	25.87	28.42	30.65	30.68	29.95	31.26
11	26.95	28.00	28.14	20.52	25.32	24.67	28.19	28.16	27.61	28.63
12	28.76	30.87	31.05	20.60	26.01	28.37	30.97	31.06	30.58	31.48
13	23.76	23.95	23.99	20.52	23.53	22.76	24.27	24.15	23.52	24.89
14	26.02	26.97	27.11	20.51	24.94	25.68	27.20	27.15	26.55	27.57
15	28.38	30.15	30.44	20.71	26.06	28.21	30.52	30.60	30.13	30.81
16	27.75	28.82	28.87	20.52	25.69	26.66	29.27	29.21	29.02	29.96
17	27.90	29.57	29.80	20.56	25.85	28.32	29.78	29.79	29.16	30.40
18	25.77	26.40	26.41	20.53	24.74	25.70	26.63	26.56	26.01	27.22
19	27.30	28.67	28.81	20.53	25.40	26.52	29.19	29.22	28.67	29.57
20	28.96	30.40	30.76	21.44	24.95	25.90	30.79	30.83	29.97	31.07
21	26.54	27.53	27.60	20.51	25.06	26.48	27.80	27.75	27.12	28.34
22	27.05	28.17	28.27	20.51	25.36	26.60	28.21	28.16	27.81	28.64
23	29.14	32.31	32.51	20.54	26.13	23.24	31.89	31.97	31.21	32.34
24	25.75	26.41	26.53	20.59	24.55	25.73	27.10	27.03	26.18	27.59
Average	27.13	28.54	28.68	20.58	25.24	26.19	28.84	28.83	28.22	29.31

Table 2. PSNR(dB) results of different denoising methods on the Kodak PhotoCD dataset.

	$\sigma_r = 30, \sigma_g = 10, \sigma_b = 50$									
Image#	CBM3D [5]	MLP [6]	TNRD [7]	DnCNN [8]	NI [9]	NC [10]	WNNM-1 [11]	WNNM-2	WNNM-3	MC-WNNM
1	23.38	26.49	26.50	20.21	24.82	23.59	26.40	25.60	24.76	27.81
2	25.19	30.94	30.90	20.43	26.82	27.79	30.89	29.75	29.21	30.96
3	25.39	32.03	32.09	20.47	27.52	27.41	32.20	31.17	30.39	32.89
4	24.96	30.55	30.47	20.34	27.34	27.00	30.74	29.71	29.10	31.19
5	23.29	26.65	26.73	20.34	25.72	26.67	26.74	25.98	24.68	27.60
6	24.09	27.76	27.70	20.45	26.10	26.12	27.85	26.96	26.01	29.15
7	24.89	30.70	30.72	20.40	27.17	28.07	30.91	29.94	28.87	31.37
8	23.30	26.12	26.27	20.32	25.59	26.11	26.87	26.33	24.74	27.44
9	25.20	31.35	31.31	20.36	27.74	28.33	31.30	30.45	29.44	32.08
10	25.13	31.01	31.05	20.38	27.60	28.53	31.12	30.17	29.21	31.83
11	24.54	28.79	28.82	20.40	26.72	24.40	28.73	27.79	26.94	29.60
12	25.43	31.60	31.60	20.44	27.82	29.01	31.59	30.62	29.91	32.11
13	22.50	24.71	24.73	20.17	24.96	23.36	24.70	23.85	22.86	25.96
14	23.91	27.69	27.72	20.34	26.26	23.08	27.62	26.81	25.91	28.57
15	25.45	31.09	31.05	20.68	27.36	28.49	31.29	30.21	29.46	31.39
16	24.89	29.79	29.73	20.39	27.35	27.10	29.84	28.85	28.13	31.10
17	25.12	30.26	30.24	20.52	27.15	27.54	30.11	29.35	28.43	31.08
18	23.83	27.26	27.26	20.39	26.05	26.15	27.32	26.18	25.28	28.32
19	24.63	29.40	29.39	20.39	27.06	27.41	29.78	28.87	28.05	30.53
20	26.43	31.16	31.27	21.39	26.43	26.92	31.25	30.43	29.41	31.55
21	24.24	28.26	28.27	20.33	26.66	27.18	28.22	27.45	26.40	29.29
22	24.51	29.03	29.06	20.33	26.83	27.64	29.02	27.81	27.18	29.57
23	25.55	32.87	32.75	20.46	27.60	23.75	32.58	31.46	30.50	32.34
24	23.85	27.06	27.13	20.37	25.86	27.05	27.50	26.63	25.55	28.32
Average	24.57	29.27	29.28	20.43	26.69	26.61	29.36	28.43	27.52	30.09

Table 3. PSNR(dB) results of different denoising methods on the Kodak PhotoCD dataset.

	$\sigma_r = 5, \sigma_g = 30, \sigma_b = 15$									
Image#	CBM3D [5]	MLP [6]	TNRD [7]	DnCNN [8]	NI [9]	NC [10]	WNNM-1 [11]	WNNM-2	WNNM-3	MC-WNNM
1	27.25	28.06	28.62	24.99	25.00	29.55	28.16	27.95	28.15	30.20
2	29.70	31.30	32.70	25.09	27.80	29.69	32.54	31.60	31.73	34.04
3	30.34	31.98	34.07	25.37	28.02	31.93	33.91	33.68	33.52	35.55
4	29.47	31.10	32.56	25.14	27.70	32.56	32.68	31.85	31.90	34.06
5	27.31	28.59	29.35	25.18	26.14	30.00	28.83	29.00	28.91	30.05
6	28.20	29.10	29.90	25.27	26.15	28.81	29.55	29.46	29.62	31.64
7	29.73	31.60	33.46	25.40	27.22	31.63	33.09	33.29	32.86	34.24
8	27.47	28.16	28.91	25.12	25.34	30.16	29.15	29.24	29.03	29.91
9	30.07	31.63	33.55	25.33	27.86	31.54	33.19	33.20	32.95	34.53
10	29.96	31.37	33.20	25.33	27.74	33.44	32.98	33.02	32.74	34.38
11	28.73	29.85	30.87	25.23	26.98	30.16	30.45	30.14	30.21	32.10
12	30.20	31.50	33.31	25.40	27.97	31.69	33.22	32.71	32.65	34.64
13	26.18	26.69	26.98	24.81	25.14	27.97	26.49	26.42	26.62	28.30
14	27.86	29.07	29.87	25.16	26.67	29.21	29.36	29.14	29.30	31.18
15	29.91	31.58	33.13	25.47	28.04	31.17	33.22	32.34	32.36	34.27
16	29.29	30.35	31.54	25.26	27.46	32.18	31.34	31.05	31.21	33.72
17	29.50	31.09	32.52	25.37	27.81	32.80	32.09	32.00	31.85	33.61
18	27.72	28.74	29.36	25.10	26.57	28.63	28.88	28.76	28.89	30.56
19	28.98	30.18	31.35	25.24	27.25	29.79	31.34	30.77	30.95	33.10
20	30.63	31.78	33.27	26.08	27.89	29.52	33.00	32.55	32.58	34.18
21	28.50	29.58	30.54	25.18	26.86	30.99	30.02	30.03	30.03	31.69
22	28.61	29.78	30.82	25.14	27.19	30.50	30.47	29.82	30.10	32.08
23	30.60	32.66	35.06	25.33	28.17	32.82	34.72	34.37	33.94	35.16
24	27.97	28.81	29.61	25.12	26.01	30.75	29.47	29.35	29.39	30.93
Average	28.92	30.19	31.44	25.26	27.04	30.73	31.17	30.91	30.89	32.67

3. More visual comparisons of denoised images on the real noisy images of dataset [1]

In this section, we give more comparisons of the state-of-the-art denoising methods on dataset [1]. The real noisy images in dataset [1] have no “ground truth” images and hence we only compare the visual quality of the denoised images by different methods. As can be seen from Figures 7-10, the proposed MC-WNNM method performs better than the competing methods.

4. More visual comparisons of denoised images on the real noisy images of dataset [2]

In this section, we provide more comparisons of the proposed method with the state-of-the-art denoising methods on the 15 cropped real noisy images used in [2]. In this dataset, each scene was shot 500 times under the same camera and camera setting. The mean image of the 500 shots is roughly taken as the “ground truth”, with which the PSNR can be computed. As can be seen from Figures 11-14, our proposed method achieves better performance than the the competing methods. This validates the effectiveness of the proposed MC-WNNM method for real noisy image denoising.

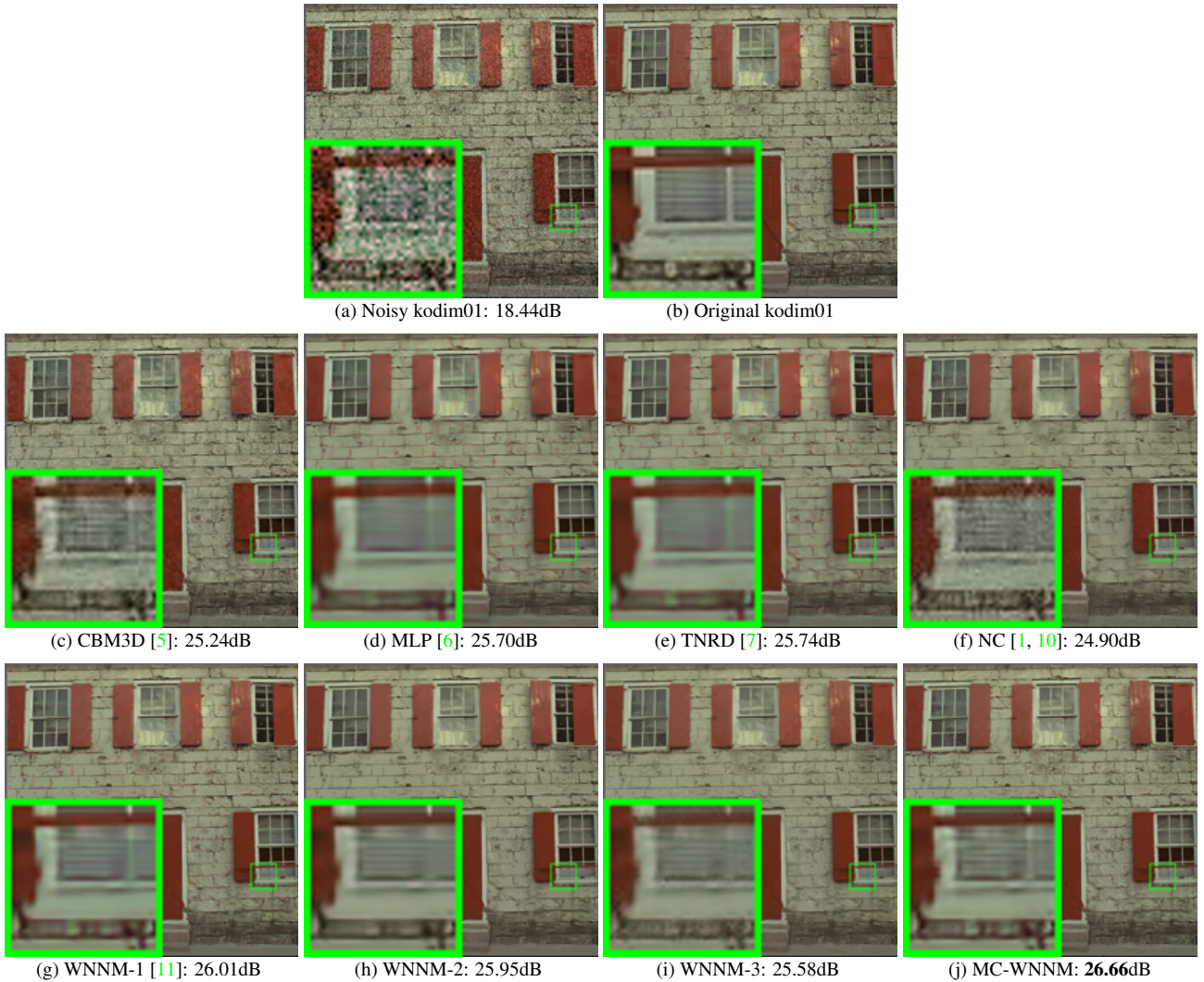


Figure 1. Denoised images of different methods on the image “kodim01” degraded by AWGN with different standard deviations of $\sigma_r = 40$, $\sigma_g = 20$, $\sigma_b = 30$ on R, G, B channels, respectively. The images are better to be zoomed in on screen.

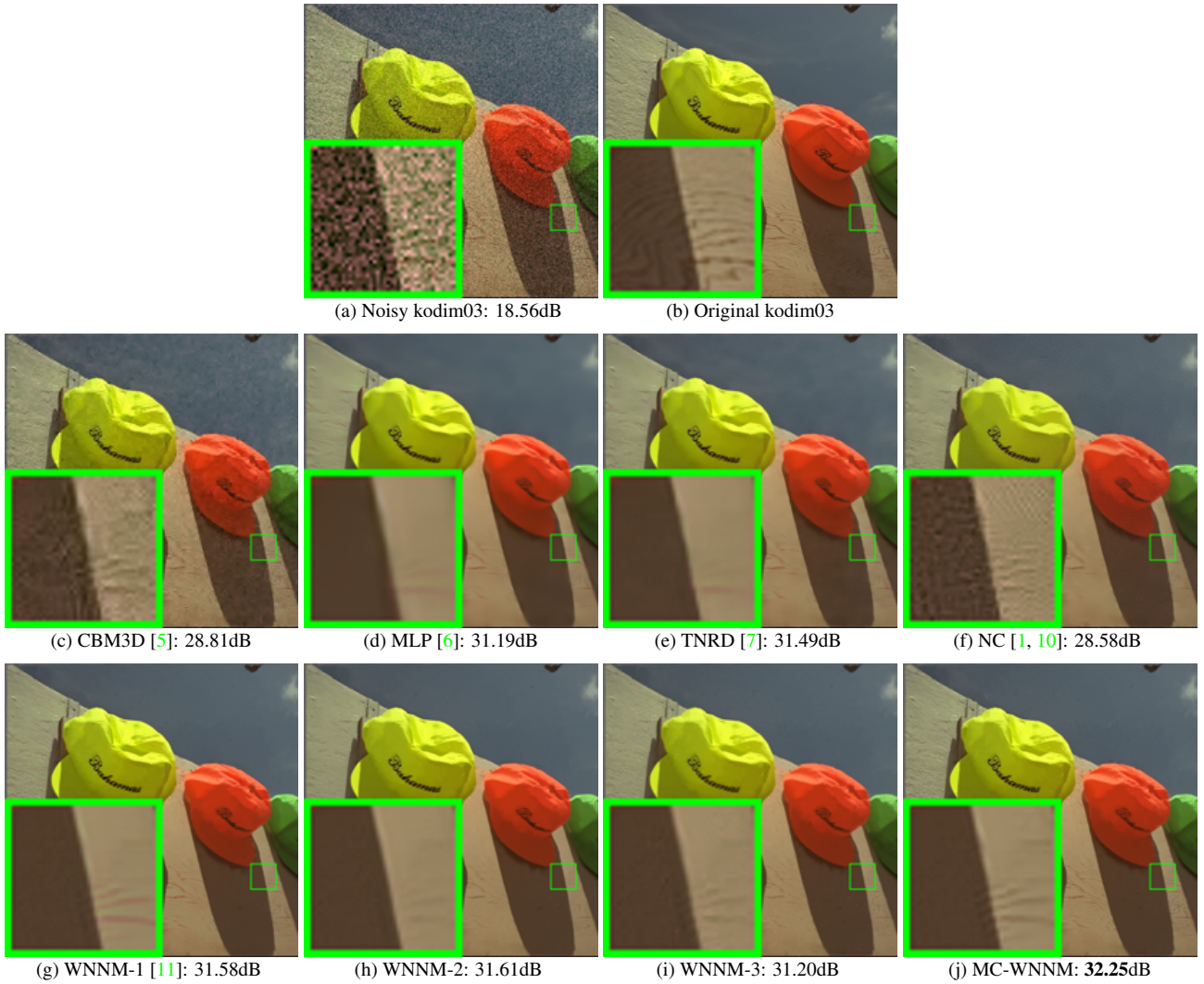


Figure 2. Denoised images of different methods on the image “kodim03” degraded by AWGN with different standard deviations of $\sigma_r = 40$, $\sigma_g = 20$, $\sigma_b = 30$ on R, G, B channels, respectively. The images are better to be zoomed in on screen.

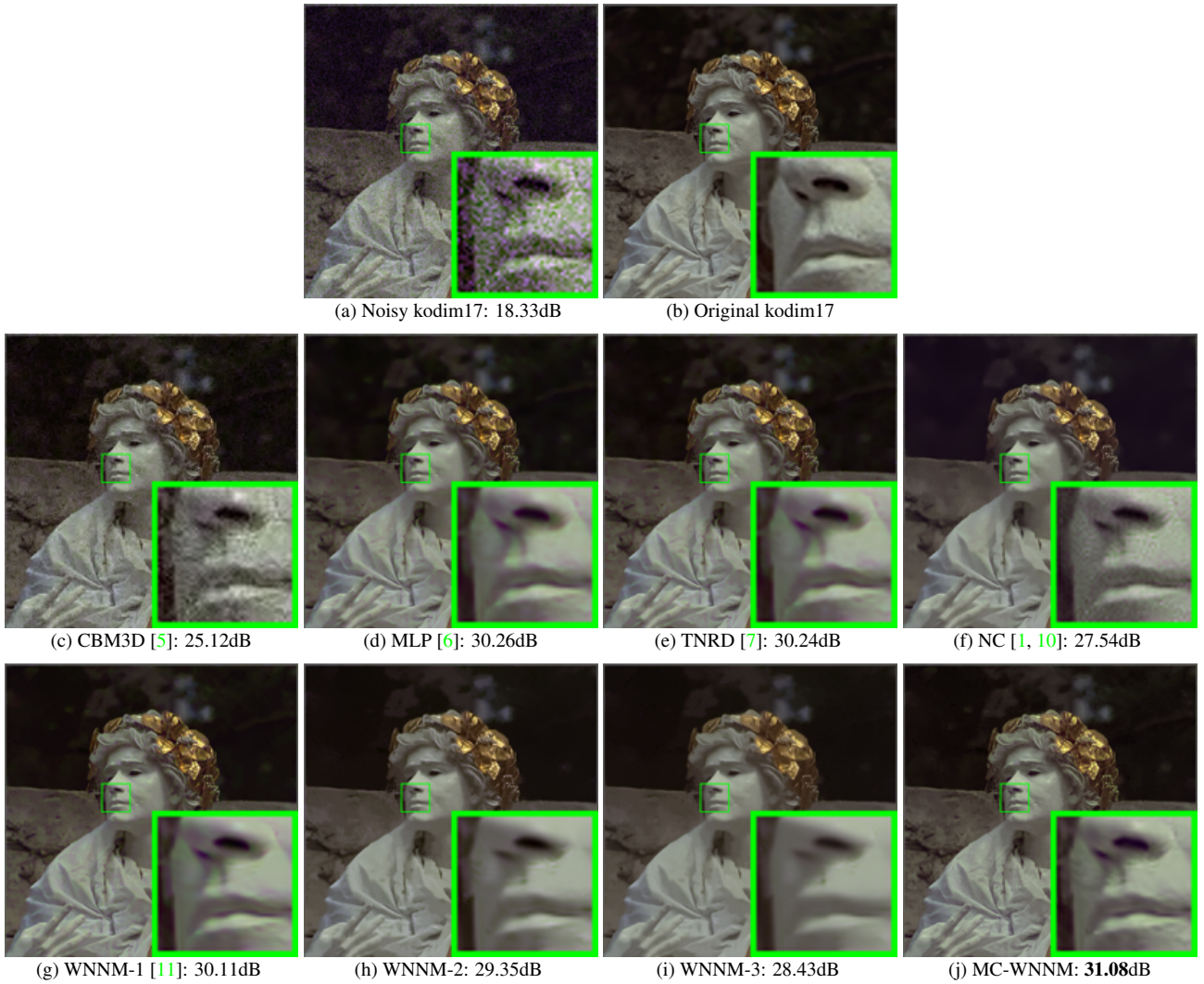


Figure 3. Denoised images of different methods on the image “kodim17” degraded by AWGN with different standard deviations of $\sigma_r = 30$, $\sigma_g = 10$, $\sigma_b = 50$ on R, G, B channels, respectively. The images are better to be zoomed in on screen.

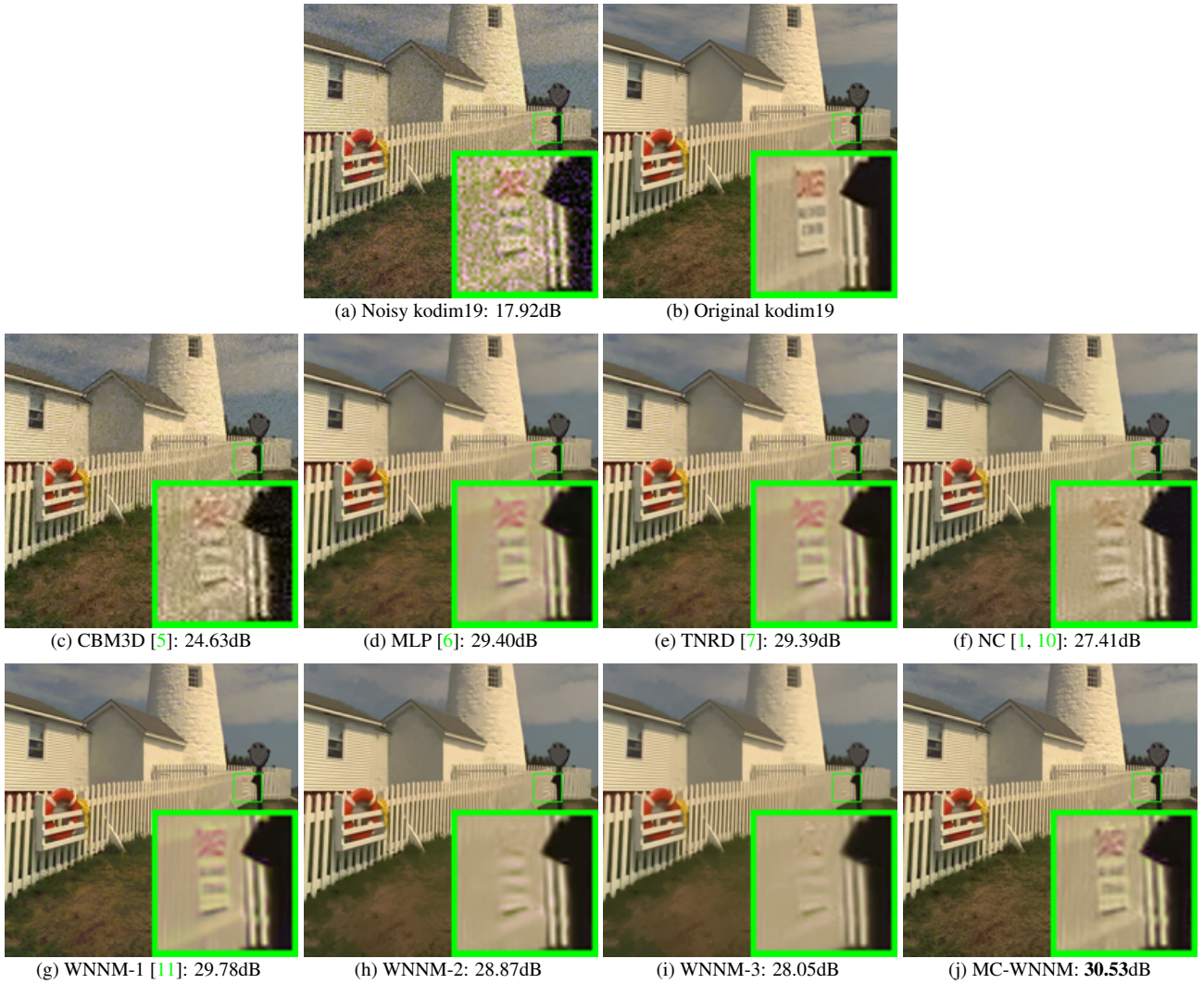


Figure 4. Denoised images of different methods on the image “kodim19” degraded by AWGN with different standard deviations of $\sigma_r = 30$, $\sigma_g = 10$, $\sigma_b = 50$ on R, G, B channels, respectively. The images are better to be zoomed in on screen.

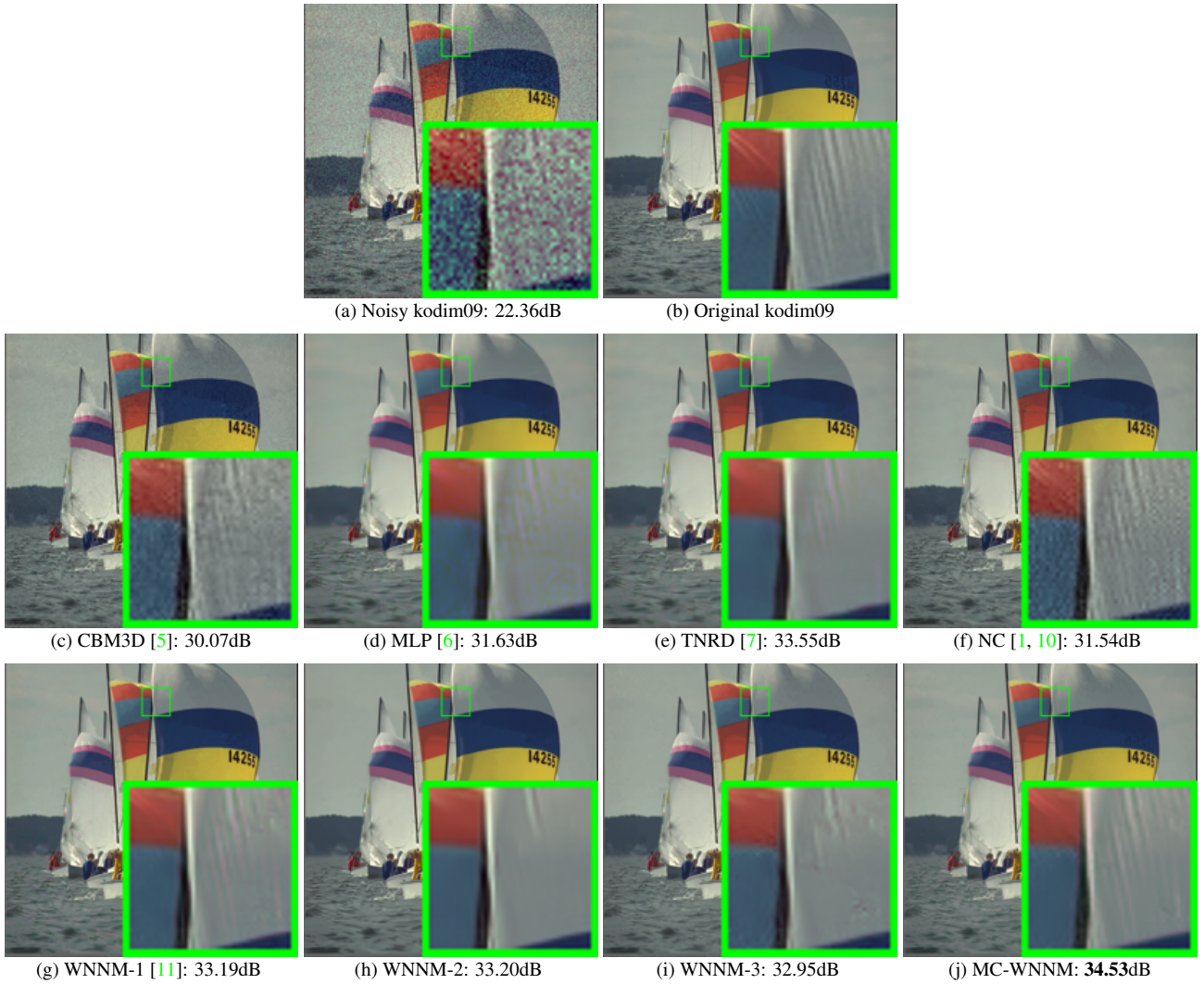


Figure 5. Denoised images of different methods on the image “kodim09” degraded by AWGN with different standard deviations of $\sigma_r = 5$, $\sigma_g = 30$, $\sigma_b = 15$ on R, G, B channels, respectively. The images are better to be zoomed in on screen.

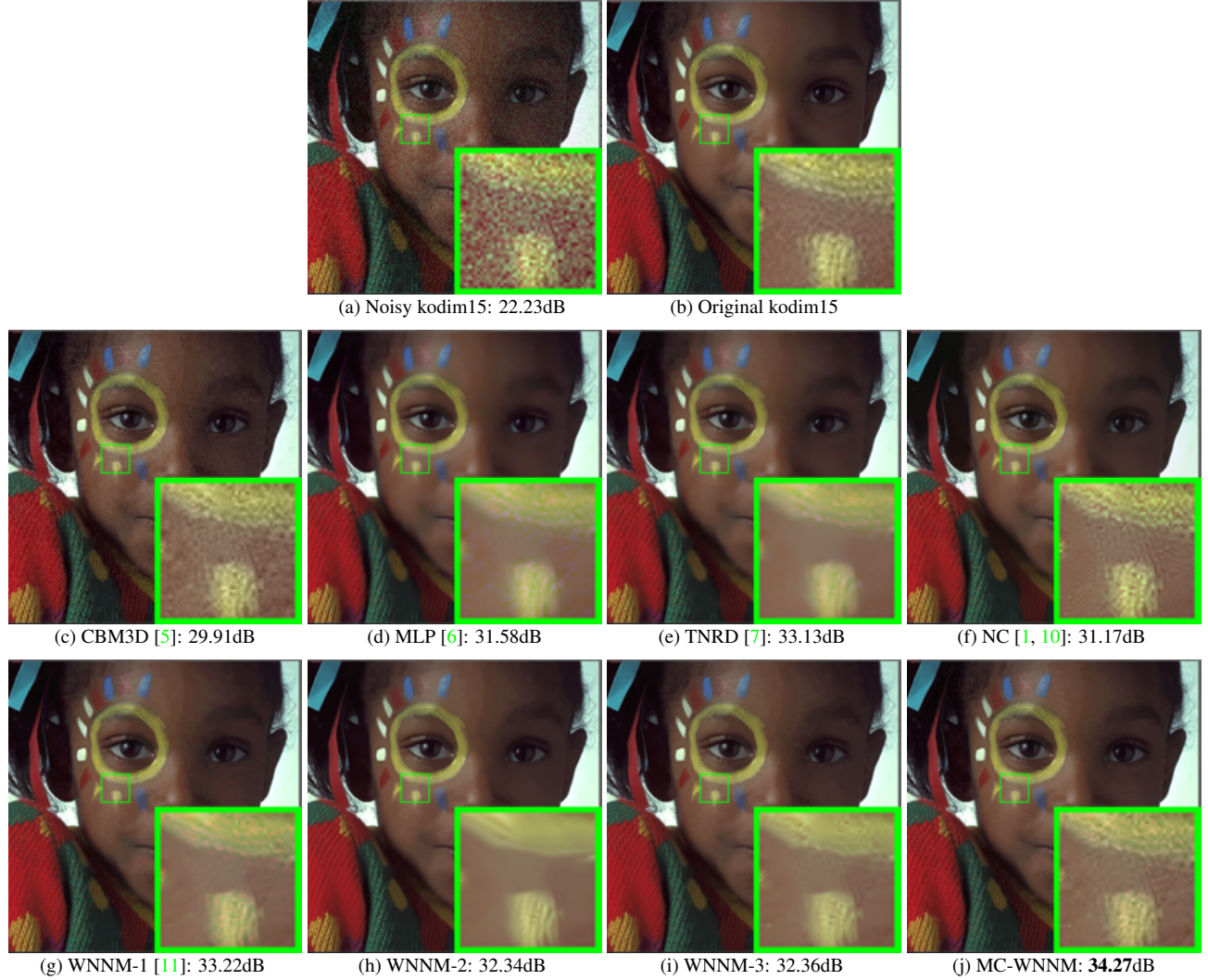


Figure 6. Denoised images of different methods on the image “kodim15” degraded by AWGN with different standard deviations of $\sigma_r = 5$, $\sigma_g = 30$, $\sigma_b = 15$ on R, G, B channels, respectively. The images are better to be zoomed in on screen.

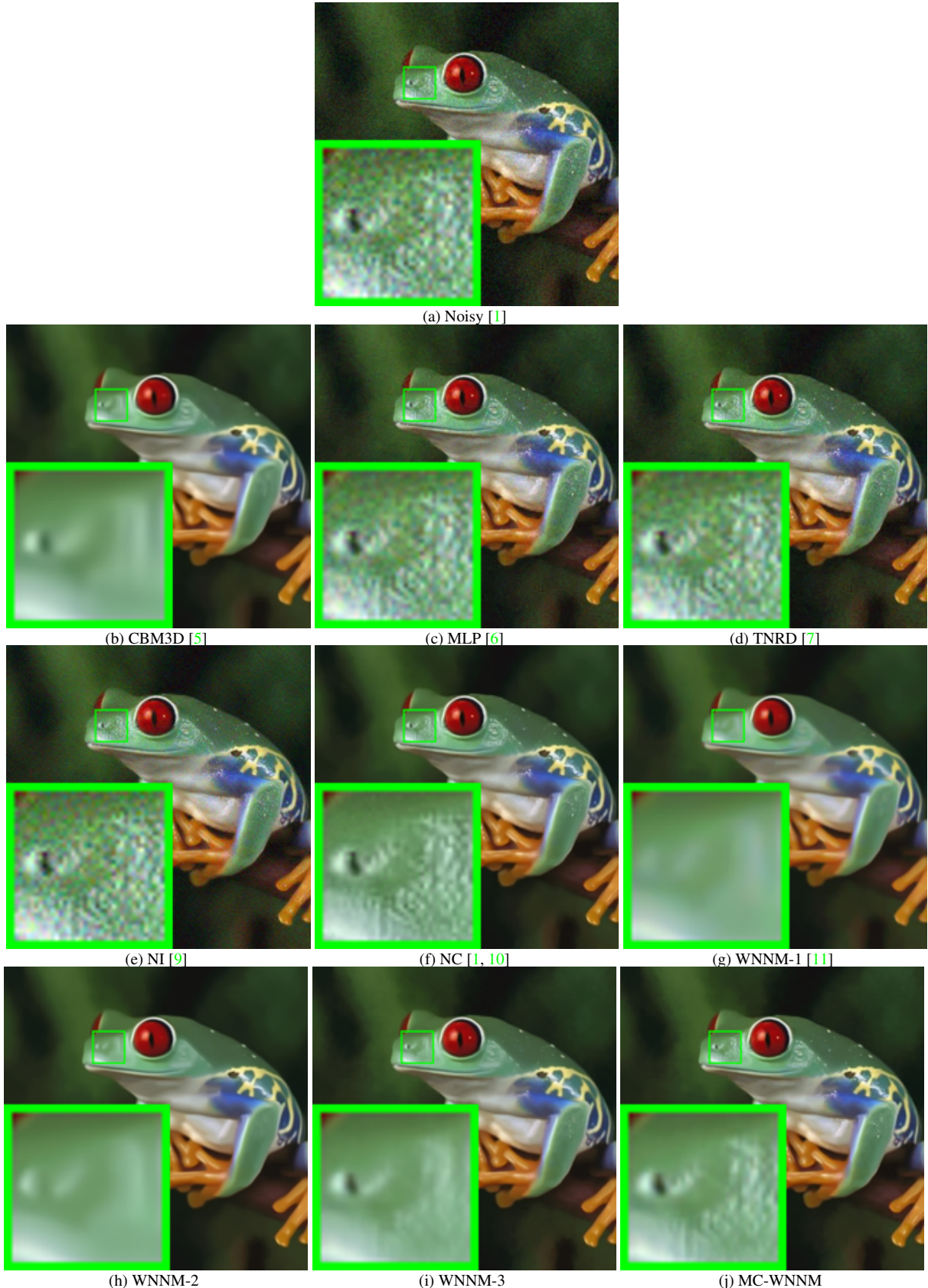


Figure 7. Denoised images of the real noisy image “Frog” [1] by different methods. The estimated noise levels of R, G, and B channels are 14.9, 15.1, and 14.6, respectively. The images are better to be zoomed in on screen.

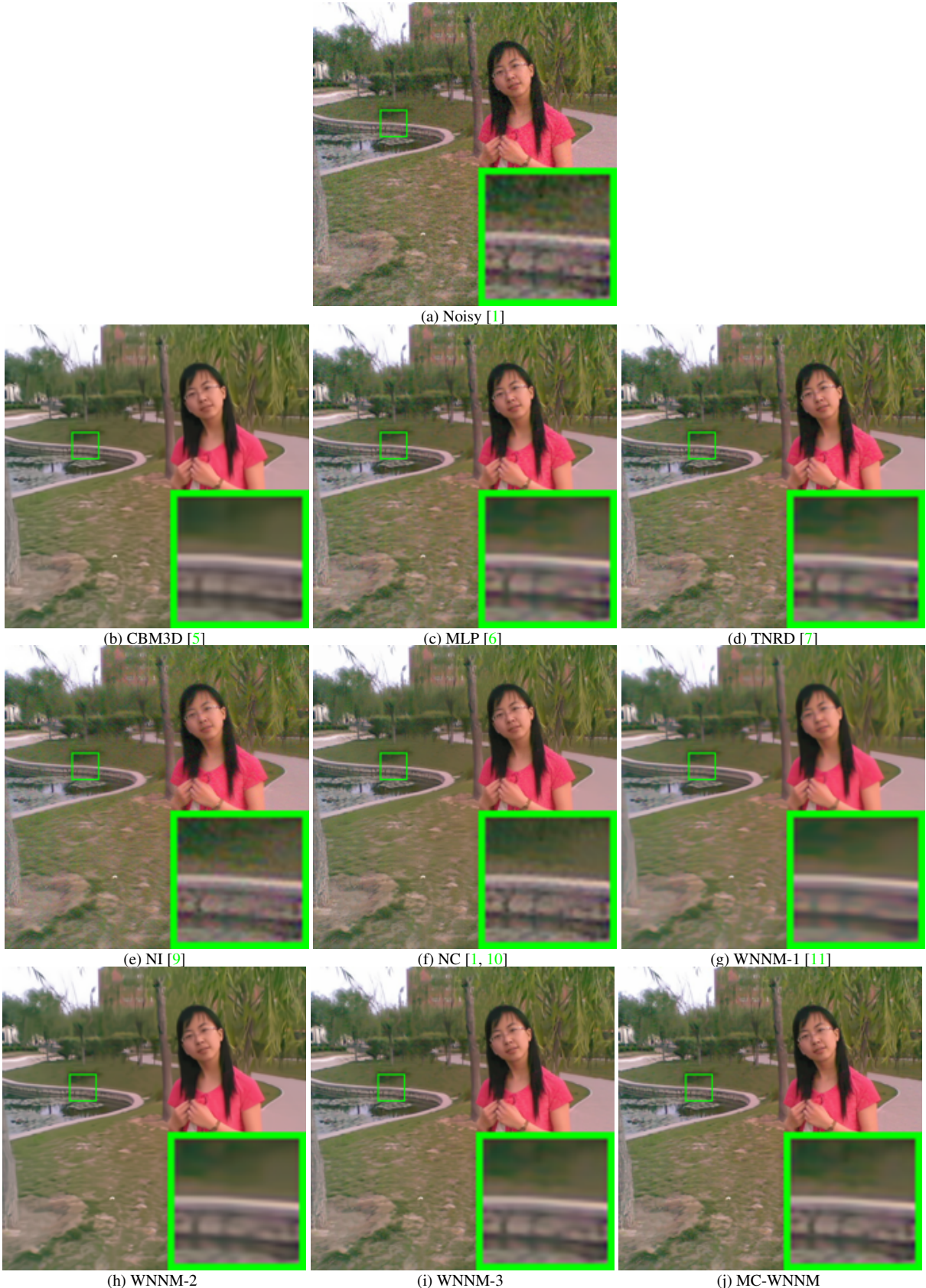


Figure 8. Denoised images of the real noisy image “Girl” [1] by different methods. The estimated noise levels of R, G, and B channels are 6.0, 6.3, and 5.8, respectively. The images are better to be zoomed in on screen.

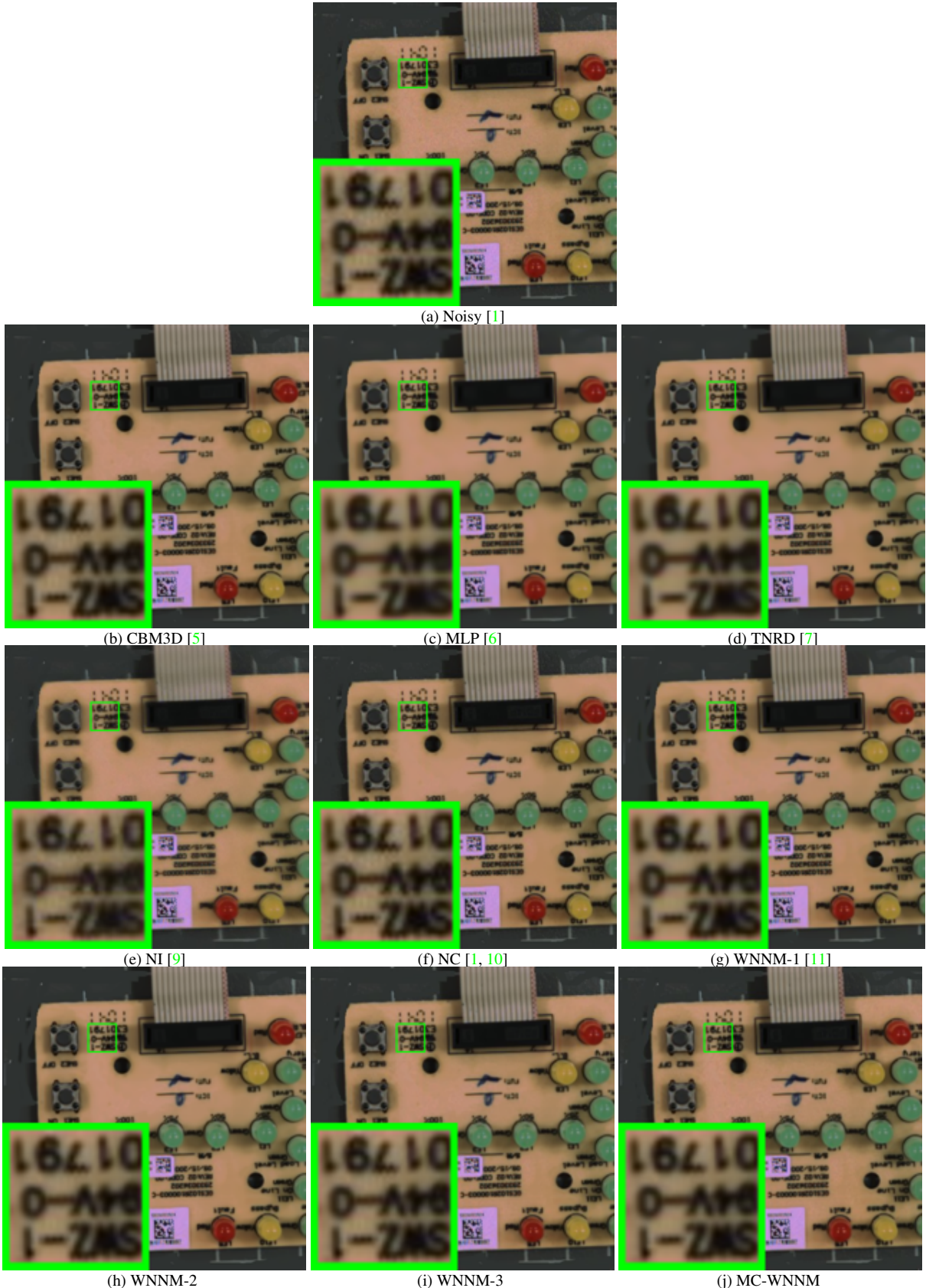


Figure 9. Denoised images of the real noisy image “Circuit” [1] by different methods. The estimated noise levels of R, G, and B channels are 1.9, 1.8, and 2.0, respectively. The images are better to be zoomed in on screen.

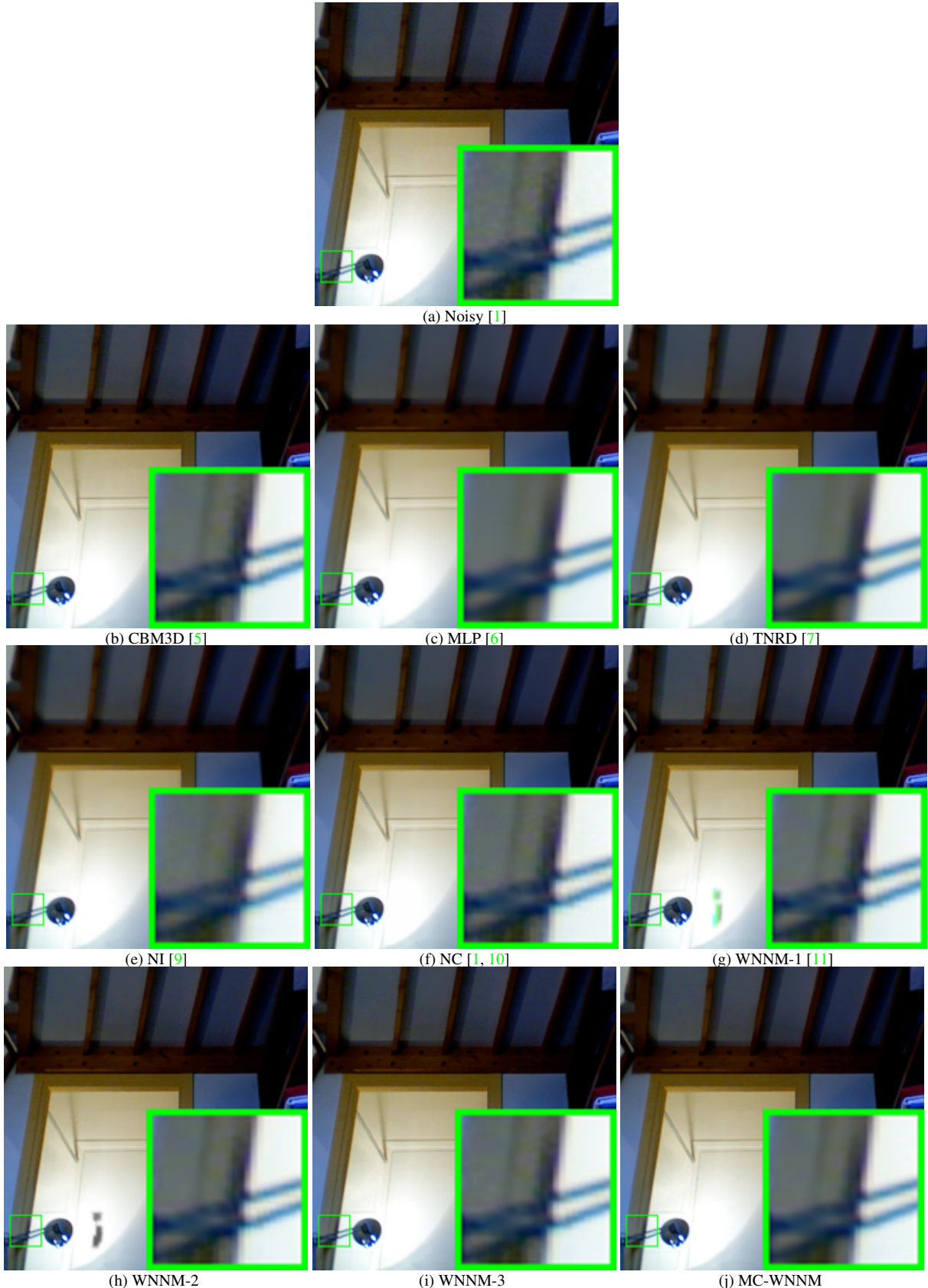


Figure 10. Denoised images of the real noisy image “Room” [1] by different methods. The estimated noise levels of R, G, and B channels are 1.4, 1.1, and 1.2, respectively. The images are better to be zoomed in on screen.

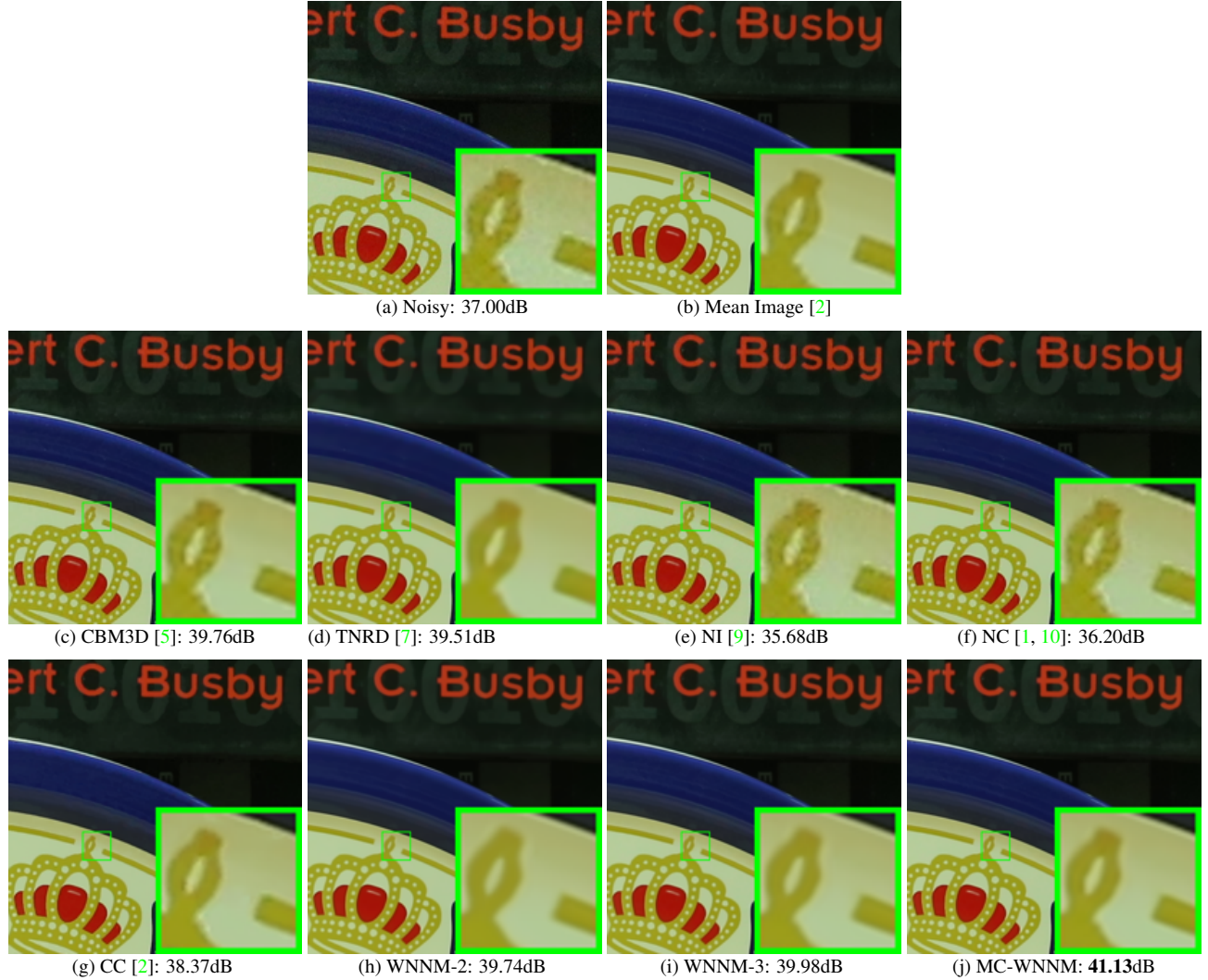


Figure 11. Denoised images of a region cropped from the real noisy image “Canon 5D Mark 3 ISO=3200 1” [2] by different methods. The estimated noise levels of R, G, and B channels are 1.6, 1.5, and 1.6, respectively. The images are better to be zoomed in on screen.

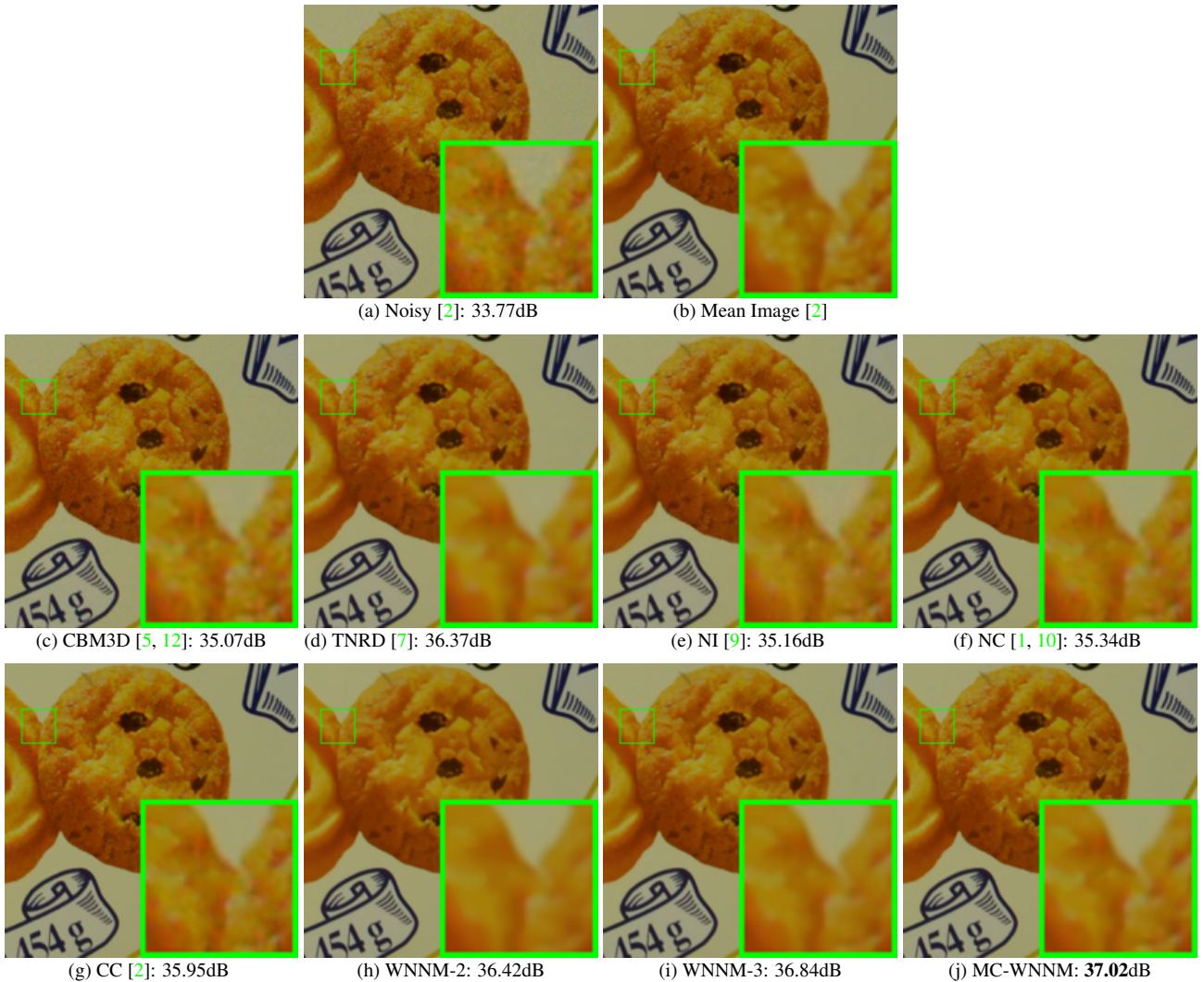


Figure 12. Denoised images of a region cropped from the real noisy image “Nikon D600 ISO=3200 2” [2] by different methods. The estimated noise levels of R, G, and B channels are 1.2, 1.3, and 1.4, respectively. The images are better to be zoomed in on screen.

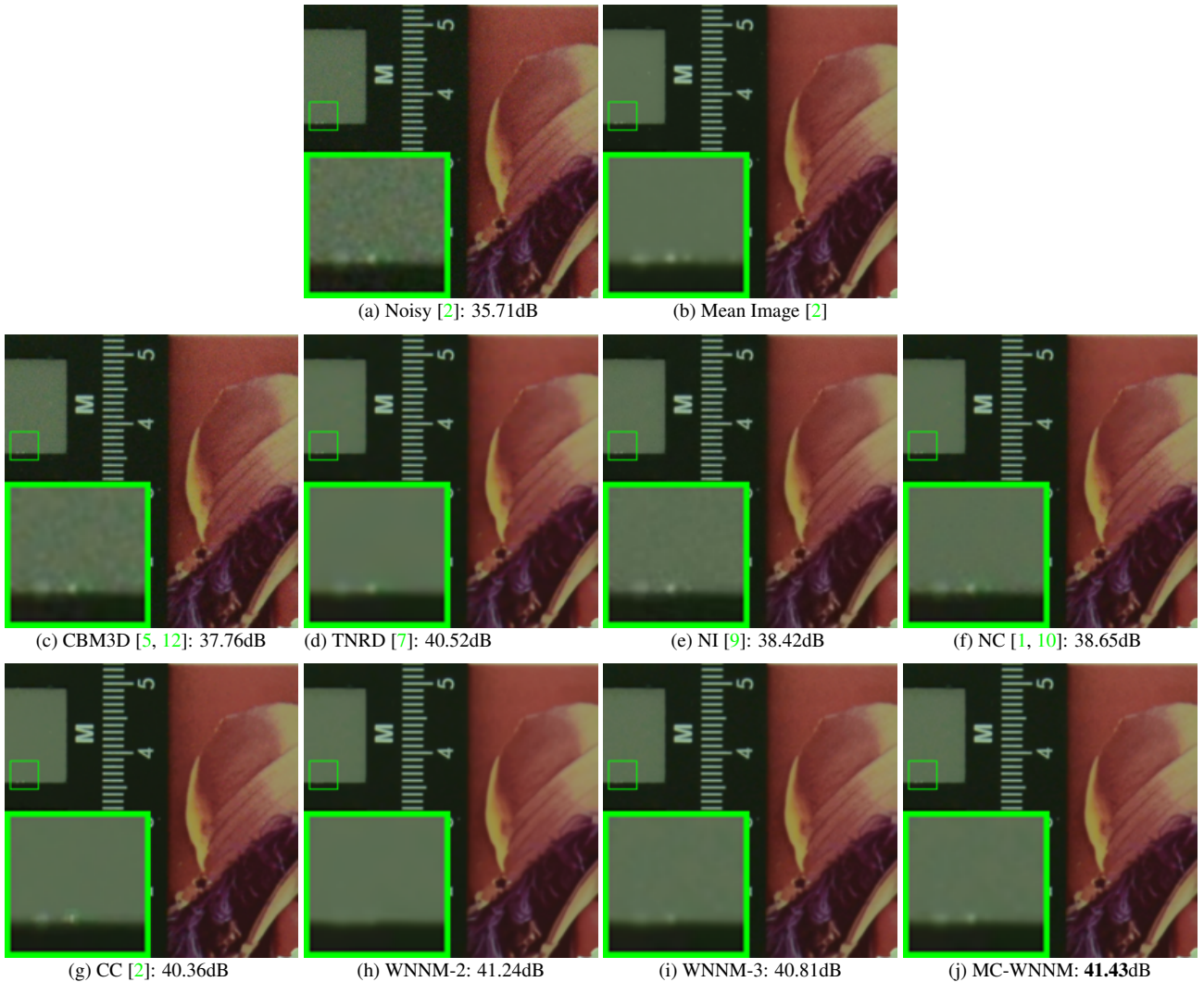


Figure 13. Denoised images of a region cropped from the real noisy image “Nikon D800 ISO=1600 2” [2] by different methods. The estimated noise levels of R, G, and B channels are 1.3, 1.1, and 1.4, respectively. The images are better to be zoomed in on screen.

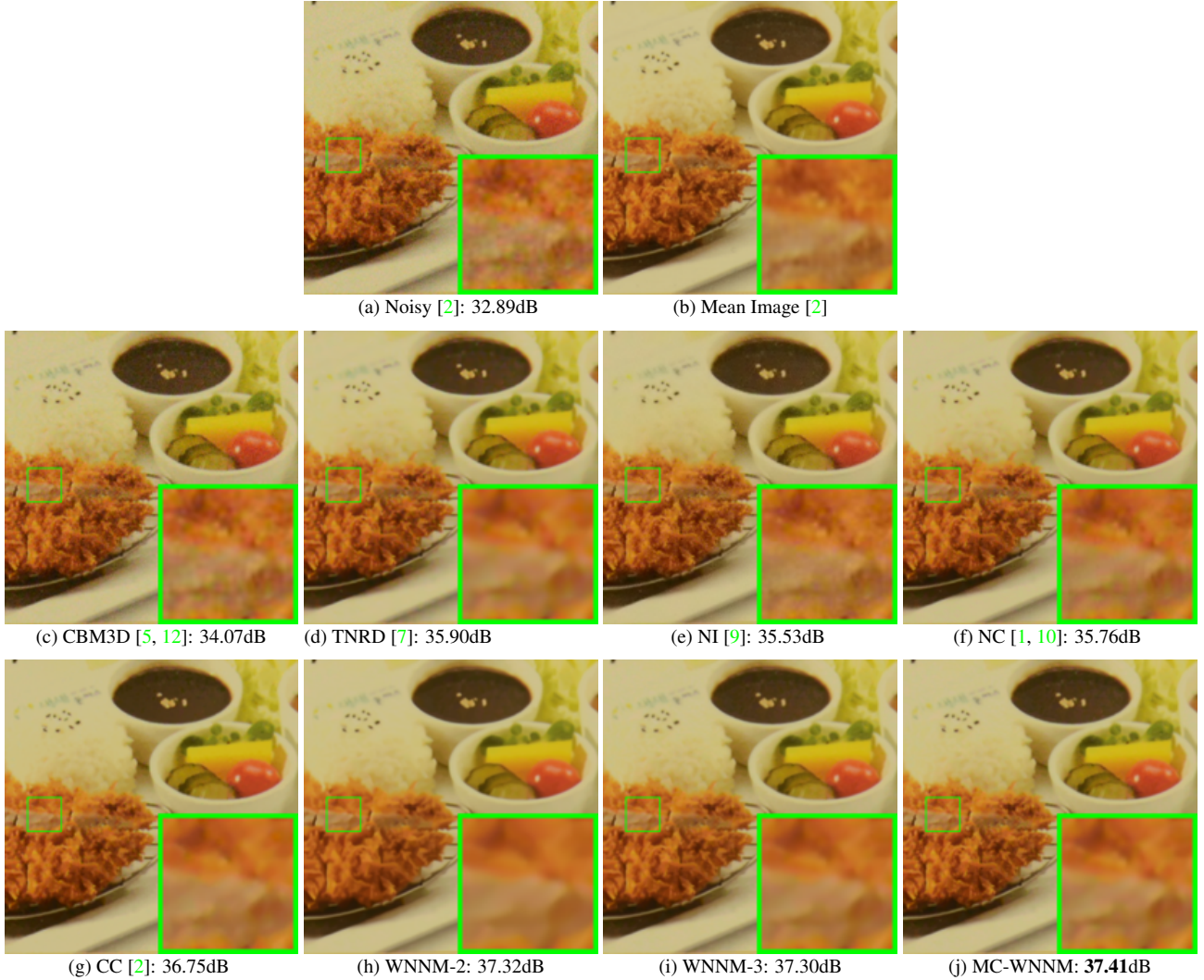


Figure 14. Denoised images of a region cropped from the real noisy image “Nikon D800 ISO=3200 2” [2] by different methods. The estimated noise levels of R, G, and B channels are 1.2, 1.0, and 1.3, respectively. The images are better to be zoomed in on screen.

References

- [1] M. Lebrun, M. Colom, and J. M. Morel. The noise clinic: a blind image denoising algorithm. <http://www.ipol.im/pub/art/2015/125/>. Accessed 01 28, 2015. 1, 4, 5, 6, 7, 8, 9, 10, 11, 12, 13, 14, 15, 16, 17, 18
- [2] S. Nam, Y. Hwang, Y. Matsushita, and S. J. Kim. A holistic approach to cross-channel image noise modeling and its application to image denoising. *IEEE Conference on Computer Vision and Pattern Recognition (CVPR)*, pages 1683–1691, 2016. 1, 4, 15, 16, 17, 18
- [3] C. Eckart and G. Young. The approximation of one matrix by another of lower rank. *Psychometrika*, 1(3):211–218, 1936. 1
- [4] S. Gu, Q. Xie, D. Meng, W. Zuo, X. Feng, and L. Zhang. Weighted nuclear norm minimization and its applications to low level vision. *International Journal of Computer Vision*, pages 1–26, 2016. 1
- [5] K. Dabov, A. Foi, V. Katkovnik, and K. Egiazarian. Color image denoising via sparse 3D collaborative filtering with grouping constraint in luminance-chrominance space. *IEEE International Conference on Image Processing (ICIP)*, pages 313–316, 2007. 3, 4, 5, 6, 7, 8, 9, 10, 11, 12, 13, 14, 15, 16, 17, 18
- [6] H. C. Burger, C. J. Schuler, and S. Harmeling. Image denoising: Can plain neural networks compete with BM3D? *IEEE Conference on Computer Vision and Pattern Recognition (CVPR)*, pages 2392–2399, 2012. 3, 4, 5, 6, 7, 8, 9, 10, 11, 12, 13, 14
- [7] Y. Chen, W. Yu, and T. Pock. On learning optimized reaction diffusion processes for effective image restoration. *IEEE Conference on Computer Vision and Pattern Recognition (CVPR)*, pages 5261–5269, 2015. 3, 4, 5, 6, 7, 8, 9, 10, 11, 12, 13, 14, 15, 16, 17, 18
- [8] K. Zhang, W. Zuo, Y. Chen, D. Meng, and L. Zhang. Beyond a gaussian denoiser: Residual learning of deep cnn for image denoising. *IEEE Transactions on Image Processing*, 2017. 3, 4
- [9] Neatlab ABSoft. Neat Image. <https://ni.neatvideo.com/home>. 3, 4, 11, 12, 13, 14, 15, 16, 17, 18
- [10] M. Lebrun, M. Colom, and J.-M. Morel. Multiscale image blind denoising. *IEEE Transactions on Image Processing*, 24(10):3149–3161, 2015. 3, 4, 5, 6, 7, 8, 9, 10, 11, 12, 13, 14, 15, 16, 17, 18
- [11] S. Gu, L. Zhang, W. Zuo, and X. Feng. Weighted nuclear norm minimization with application to image denoising. *IEEE Conference on Computer Vision and Pattern Recognition (CVPR)*, pages 2862–2869, 2014. 3, 4, 5, 6, 7, 8, 9, 10, 11, 12, 13, 14
- [12] K. Dabov, A. Foi, V. Katkovnik, and K. Egiazarian. Image denoising by sparse 3-D transform-domain collaborative filtering. *IEEE Transactions on Image Processing*, 16(8):2080–2095, 2007. 16, 17, 18